TU Delft

Neural networks with physical constraints

Domain decomposition-based network architectures and model order reduction

Alexander Heinlein[1]

NVIDIA/HLRS SciML GPU Bootcamp, Online, April 26-27, 2023

[1]Delft University of Technology

Scientific Machine Learning in Computational Science and Engineering

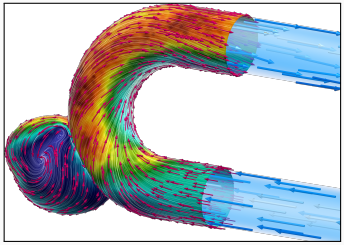
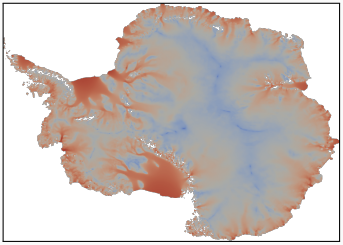
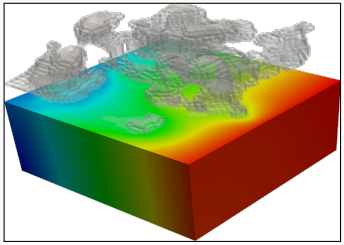

Numerical methods

Based on physical models

+ Robust and generalizable
− Require availability of mathematical models

Machine learning models

Driven by data

+ Do not require mathematical models
− Sensitive to data, limited extrapolation capabilities

Scientific machine learning (SciML)

Combining the strengths and **compensating the weaknesses** of the individual approaches:

numerical methods	**improve**	machine learning techniques
machine learning techniques	**assist**	numerical methods

Scientific Machine Learning as a Standalone Field

N. Baker, A. Frank, T. Bremer, A. Hagberg, Y. Kevrekidis, H. Najm, M. Parashar, A. Patra, J. Sethian, S. Wild, K. Willcox, and S. Lee.

Workshop Report on Basic Research Needs for Scientific Machine Learning: Core Technologies for Artificial Intelligence.

USDOE Office of Science (SC), Washington, DC (United States), 2019.

Priority Research Directions

Foundational research themes:

- Domain-awareness
- Interpretability
- Robustness

Capability research themes:

- Massive scientific data analysis
- Machine learning-enhanced modeling and simulation
- Intelligent automation and decision-support for complex systems

Development of the Field of Scientific Machine Learning

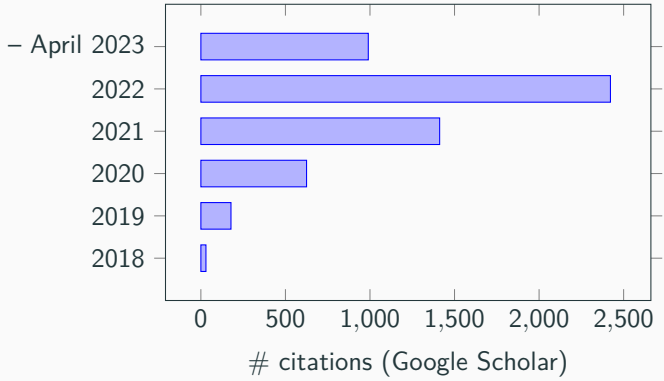

M. Raissi, P. Perdikaris, and G. E. Karniadakis.
Physics-informed neural networks: A deep learning framework for solving forward and inverse problems involving nonlinear partial differential equations.
Journal of Computational physics, 378, 686-707. 2019.

(and the respective arXiv preprints)

Scientific Machine Learning Examples

Many approaches in scientific machine learning have been developed in the past few years.

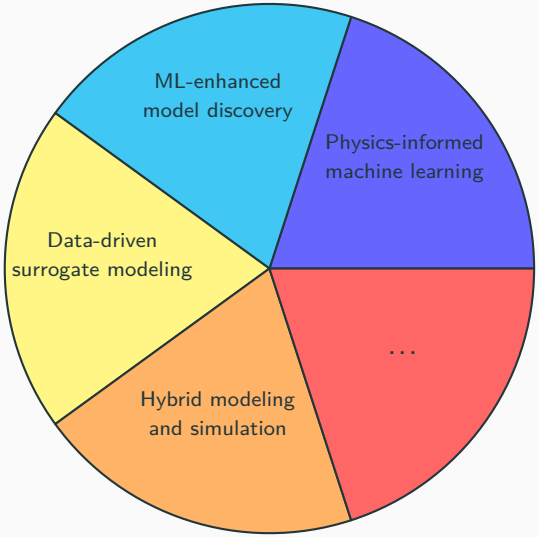

Scientific Machine Learning Examples

Many approaches in scientific machine learning have been developed in the past few years. We will focus on **two types**:

Data-driven surrogate modeling

Replacing a **computationally expensive** numerical simulator by a **fast** data-driven model.

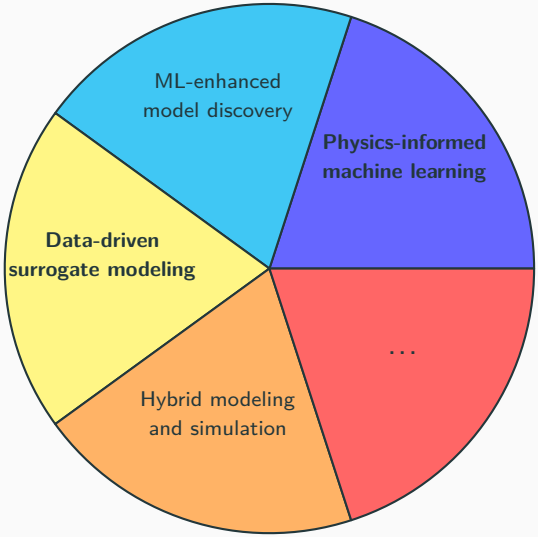

Physics-informed machine learning

Regularizing a data-driven machine learning model using a physics-based model.

Outline

1. Physics-informed machine learning

2. Domain decomposition-based network architectures for physics-informed neural networks

   Based on joint work with

   Victorita Dolean (University of Strathclyde, University Côte d'Azur)

   Ben Moseley and **Siddhartha Mishra** (ETH Zürich)

3. Surrogate models for computational fluid dynamics simulations

   Based on joint work with

   Mattias Eichinger, **Viktor Grimm**, and **Axel Klawonn** (University of Cologne)

Physics-informed machine learning

Artificial Neural Networks for Solving Ordinary and Partial Differential Equations

Isaac Elias Lagaris, Aristidis Likas, *Member, IEEE,* and Dimitrios I. Fotiadis

Published in IEEE TRANSACTIONS ON NEURAL NETWORKS, VOL. 9, NO. 5, 1998.

Approach

Solve a general differential equation subject to boundary conditions

$$G(\boldsymbol{x}, \Psi(\boldsymbol{x}), \nabla\Psi(\boldsymbol{x}), \nabla^2\Psi(\boldsymbol{x})) = 0 \quad \text{in } \Omega$$

by solving an **optimization problem**

$$\min_{\theta} \sum_{x_i} G(\boldsymbol{x}_i, \Psi_t(\boldsymbol{x}_i, \theta), \nabla\Psi_t(\boldsymbol{x}_i, \theta), \nabla^2\Psi_t(\boldsymbol{x}_i, \theta))^2$$

where $\Psi_t\big(\boldsymbol{x}, \theta\big)$ is a **trial function**, $\boldsymbol{x}_i$ **sampling points inside the domain** Ω and θ are **adjustable parameters**.

Construction of the trial functions

The trial functions **explicitly satisfy the boundary conditions**:

$$\Psi_t(\boldsymbol{x}, \mathbf{p}) = A(\boldsymbol{x}) + F(\boldsymbol{x}, N(\boldsymbol{x}, \mathbf{p}))$$

- N is a **feedforward neural network** with **trainable parameters** θ and input $x \in \mathbb{R}^n$
- A and F are **fixed functions**, chosen s.t.:
  - A **satisfies the boundary conditions**
  - F **does not contribute to the boundary conditions**

Neural Networks for Solving Differential Equations

Approach

Solve a general differential equation subject to boundary conditions

$$G(\boldsymbol{x}, \Psi(\boldsymbol{x}), \nabla\Psi(\boldsymbol{x}), \nabla^2\Psi(\boldsymbol{x})) = 0 \quad \text{in } \Omega$$

by solving an **optimization problem**

$$\min_{\theta} \sum_{\boldsymbol{x}_i} G(\boldsymbol{x}_i, \Psi_t(\boldsymbol{x}_i, \theta), \nabla\Psi_t(\boldsymbol{x}_i, \theta), \nabla^2\Psi_t(\boldsymbol{x}_i, \theta))^2$$

where $\Psi_t(\boldsymbol{x}, \theta)$ is a **trial function**, $\boldsymbol{x}_i$ **sampling points inside the domain** Ω and θ are **adjustable parameters**.

Construction of the trial functions

The trial functions **explicitly satisfy the boundary conditions**:

$$\Psi_t(\boldsymbol{x}, \mathbf{p}) = A(\boldsymbol{x}) + F(\boldsymbol{x}, N(\boldsymbol{x}, \mathbf{p}))$$

- N is a **feedforward neural network** with **trainable parameters** θ and input $x \in \mathbb{R}^n$
- A and F are **fixed functions**, chosen s.t.:
  - A **satisfies the boundary conditions**
  - F **does not contribute to the boundary conditions**

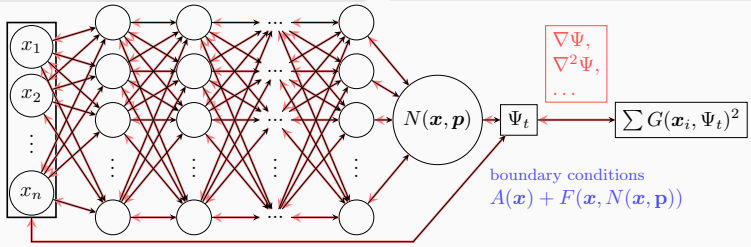

Physics-Informed Neural Networks (PINNs)

In the **physics-informed neural network (PINN)** approach introduced by Raissi et al. (2019), a **neural network** is employed to **discretize a partial differential equation**

$$\mathcal{N}[u](\boldsymbol{x},t) \quad = \quad f(\boldsymbol{x},t), \qquad (\boldsymbol{x},t) \in [0,T] \times \Omega \subset \mathbb{R}^d.$$

It is based on the approach by Lagaris et al. (1998). The main novelty of PINNs is the use of a **hybrid loss function**:

$$\mathcal{L} = \omega_{\text{data}}\mathcal{L}_{\text{data}} + \omega_{\text{PDE}}\mathcal{L}_{\text{PDE}},$$

where ω_{data} and ω_{PDE} are **weights** and

$$\mathcal{L}_{\text{data}} \quad = \quad \frac{1}{N_{\text{data}}} \sum_{i=1}^{N_{\text{data}}} \left(u(\hat{\boldsymbol{x}}_i, \hat{\boldsymbol{t}}_i) - u_i \right)^2,$$

$$\mathcal{L}_{\text{PDE}} \quad = \quad \frac{1}{N_{\text{PDE}}} \sum_{i=1}^{N_{\text{PDE}}} \left(\mathcal{N}[u](\boldsymbol{x}_i, \boldsymbol{t}_i) - f(\boldsymbol{x}_i, \boldsymbol{t}_i) \right)^2.$$

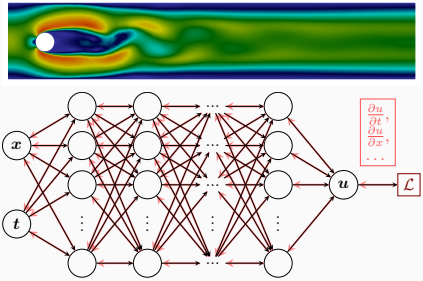

Hybrid loss

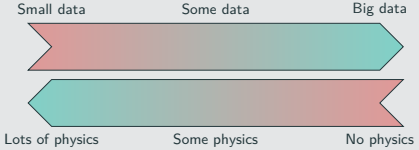

- **Known solution values** can be included in $\mathcal{L}_{\text{data}}$
- **Initial and boundary conditions** are also included in $\mathcal{L}_{\text{data}}$

Advantages

- "Meshfree"
- Small data
- Generalization properties
- High-dimensional problems
- Inverse and parameterized problems

Drawbacks

- Training cost and robustness
- Convergence not well-understood
- Difficulties with scalability and multi-scale problems

Available Theoretical Results for PINNs – An Example

Mishra and Molinaro. *Estimates on the generalisation error of PINNs*, **2022**

Estimate of the generalization error

The generalization error (or total error) satisfies

$$\mathcal{E}_G \leq C_{\text{PDE}} \mathcal{E}_T + C_{\text{PDE}} C_{\text{quad}}^{1/p} N^{-\alpha/p}$$

where

- $\mathcal{E}_G = \mathcal{E}_G(\theta; \boldsymbol{X}) := \|\mathbf{u} - \mathbf{u}^*\|_V$ (V Sobolev space, $\boldsymbol{X}$ training data set)
- $\mathcal{E}_T$ is the training error (l^p loss of the residual of the PDE)
- C_{PDE} and C_{quad} constants depending on the PDE resp. the quadrature
- N number of the training points and α convergence rate of the quadrature

Rule of thumb:

> **"As long as the PINN is trained well, it also generalizes well"**

Scaling Issues in Neural Network Training

- **Spectral bias: neural networks prioritize learning lower frequency functions** first irrespective of their amplitude

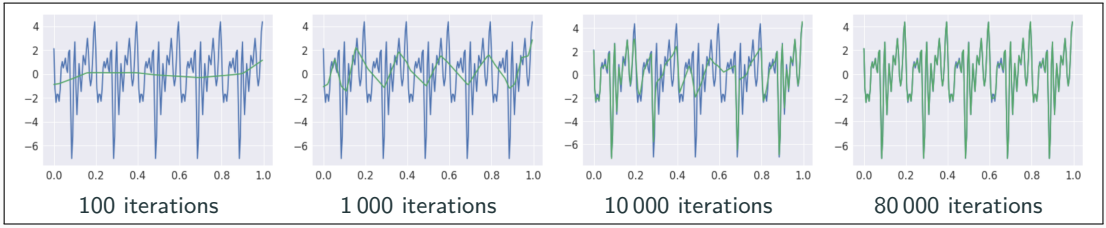

Rahaman et al., *On the spectral bias of neural networks*, **ICML (2019)**

- Solving solutions on **large domains and/or with multiscale features** potentially requires **very large neural networks**.
- Training may **not sufficiently reduce the loss** or take **large numbers of iterations**.
- Significant **increase on the computational work**

Convergence analysis of PINNs via the **neural tangent kernel**: **Wang, Yu, Perdikaris,** *When and why PINNs fail to train: A neural tangent kernel perspective*, **JCP (2022)**

Domain decomposition-based network architectures for physics-informed neural networks

Motivation – Some Observations on the Performance of PINNs

Solve

$$\begin{aligned} u' &= \cos(\omega x), \\ u(0) &= 0, \end{aligned}$$

for different values of ω using **PINNs with varying network capacities**.

Scaling issues

- Large computational domains
- Small frequencies

Cf. **Moseley, Markham, and Nissen-Meyer (arXiv 2021)**

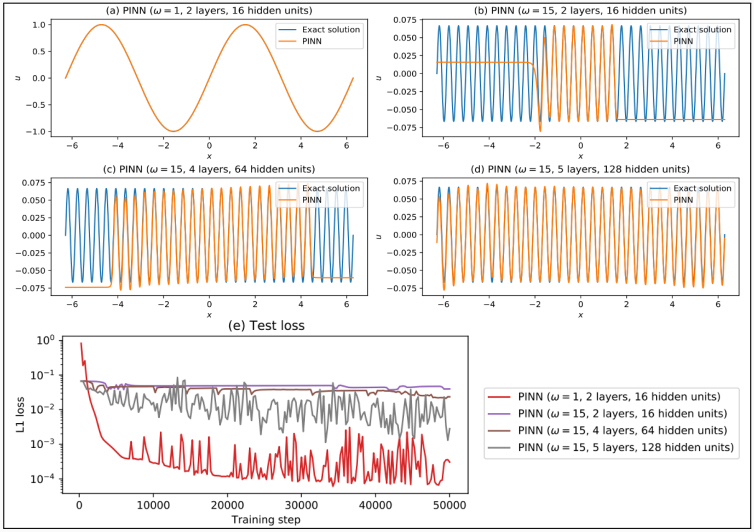

(a) 321 free parameters (d) 66 433 free parameters

Domain Decomposition Methods

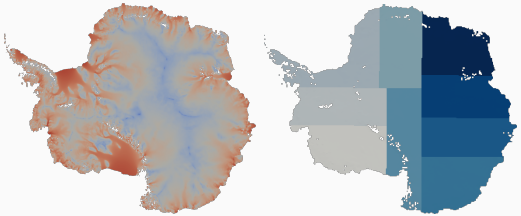

Images based on Heinlein, Perego, Rajamanickam (2022)

Idea

Decomposing a large **global problem** into smaller **local problems**:

- Better **robustness** and **scalability** of numerical solvers
- Improved **computational efficiency**
- Introduce **parallelism**

Historical remarks: The **alternating Schwarz method** is the earliest **domain decomposition method (DDM)**, which has been invented by **H. A. Schwarz** and published in **1870**:

- Schwarz used the algorithm to establish the **existence of harmonic functions** with prescribed boundary values on **regions with non-smooth boundaries**.

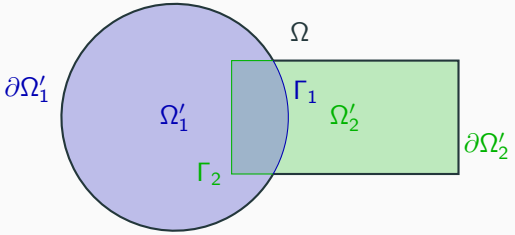

Machine Learning and Domain Decomposition Methods

A **non-exhaustive overview**:

- **Machine Learning for adaptive BDDC, FETI–DP, and AGDSW**: Heinlein, Klawonn, Lanser, Weber (2019, 2020, 2021, 2021, 2021, 2022); Klawonn, Lanser, Weber (preprint 2022)
- **Domain decomposition for CNNs**: Gu, Zhang, Liu, Cai (2022); Lee, Park, Lee (2022); Klawonn, Lanser, Weber (arXiv 2023)
- **D3M**: Li, Tang, Wu, and Liao (2019)
- **DeepDDM**: Li, Xiang, Xu (2020); Mercier, Gratton, Boudier (arXiv 2021); Li, Wang, Cui, Xiang, Xu (2023)
- **FBPINNs**: Moseley, Markham, and Nissen-Meyer (arXiv 2021); Dolean, Heinlein, Mishra, Moseley (accepted 2023, in preparation)
- **Schwarz Domain Decomposition Algorithm for PINNs**: Kim, Yang (2022, arXiv 2022)
- **cPINNs**: Jagtap, Kharazmi, Karniadakis (2020)
- **XPINNs**: Jagtap, Karniadakis (2020)

An overview of the state-of-the-art in early 2021:

A. Heinlein, A. Klawonn, M. Lanser, J. Weber.

Combining machine learning and domain decomposition methods for the solution of partial differential equations — A review.

GAMM-Mitteilungen. 2021.

Finite Basis Physics-Informed Neural Networks (FBPINNs)

In the **finite basis physics informed neural network (FBPINNs) method** introduced in Moseley, Markham, and Nissen-Meyer (arXiv 2021), we solve the boundary value problem

$$\begin{aligned} \mathcal{N}[u](\boldsymbol{x}) &= f(\boldsymbol{x}), & \boldsymbol{x} \in \Omega \subset \mathbb{R}^d, \\ \mathcal{B}_k[u](\boldsymbol{x}) &= g_k(\boldsymbol{x}), & \boldsymbol{x} \in \Gamma_k \subset \partial\Omega. \end{aligned}$$

using the **PINN** approach and **hard enforcement of the boundary conditions**, similar to Lagaris et al. (1998).

FBPINNs use the **network architecture**

$$u(\theta_1, \ldots, \theta_J) = \mathcal{C} \sum_{j=1}^{J} \omega_j u_j(\theta_j)$$

and the **loss function**

$$\mathcal{L}(\theta_1, \ldots, \theta_J) = \frac{1}{N} \sum_{i=1}^{N} \left(\mathcal{N}[\mathcal{C} \sum_{\boldsymbol{x}_i \in \Omega_j} \omega_j u_j](\boldsymbol{x}_i, \theta_j) - f(\boldsymbol{x}_i) \right)^2.$$

- **Overlapping DD**: $\Omega = \bigcup_{l=1}^{J} \Omega_j$
- **Window functions** ω_j with $\mathrm{supp}(\omega_j) \subset \Omega_j$ and $\sum_{j=1}^{J} \omega_j \equiv 1$ on Ω

Hard enforcement of boundary conditions

Loss function

$$\mathcal{L}(\theta) = \frac{1}{N} \sum_{i=1}^{N} (\mathcal{N}[\mathcal{C}u](\boldsymbol{x}_i, \theta) - f(\boldsymbol{x}_i))^2,$$

with constraining operator $\mathcal{C}$, which **explicitly enforces the boundary conditions**.

→ Often **improves training performance**

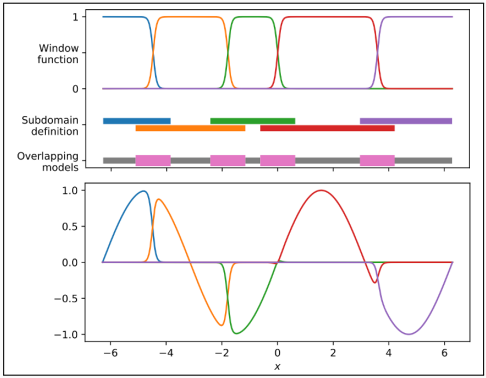

Numerical Results for FBPINNs

PINN Vs FBPINN (Moseley et al. (arXiv 2021))

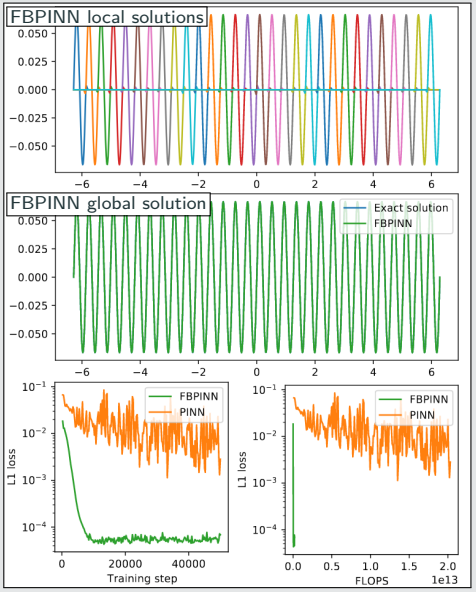

Scalability of FBPINNs

Consider the **simple boundary value problem**

$$-u'' = 1 \quad \text{in } [0,1],$$

$$u(0) = u(1) = 0,$$

which has the **solution**

$$u(x) = 1/2 x(1-x).$$

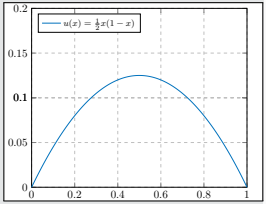

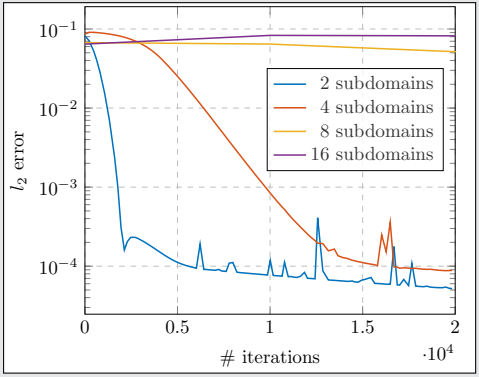

Two-Level FBPINN Algorithm

Coarse correction and spectral bias

Questions:

- Scalability requires **global transport of information**. This can be done via **coarse global problem**.
- What does this mean in the **context of network training**?

Idea:

→ Learn **low frequencies** using a **small global network**, train **high frequencies** using **local networks**.

Two-level FBPINN network architecture:

$$u(\theta_0, \theta_1, \dots, \theta_J) = \mathcal{C}\left(u_0(\theta_0) + \sum_{j=1}^{J} \omega_j u_j(\theta_j)\right)$$

Consider a **simple model problem** with **two frequencies**

$$\begin{cases} u' &= \omega_1 \cos(\omega_1 x) + \omega_2 \cos(\omega_2 x) \\ u(0) &= 0. \end{cases}$$

with $\omega_1 = 1$, $\omega_2 = 15$.

Cf. **Dolean, Heinlein, Mishra, Moseley (accepted 2023)**.

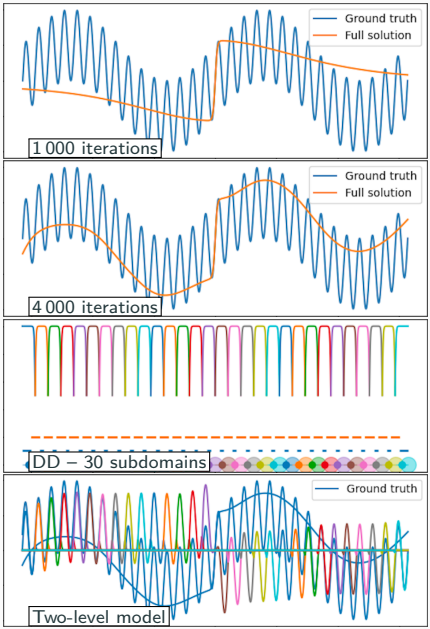

Numerical Results for FBPINNs – One Versus Two Levels

Consider, again, the **simple boundary value problem**

$$-u'' = 1 \quad \text{in } [0,1],$$
$$u(0) = u(1) = 0,$$

which has the **solution**

$$u(x) = 1/2 x(1-x).$$

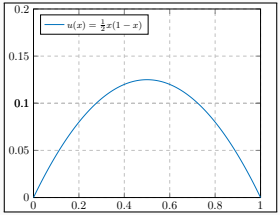

One-Level FBPINNs

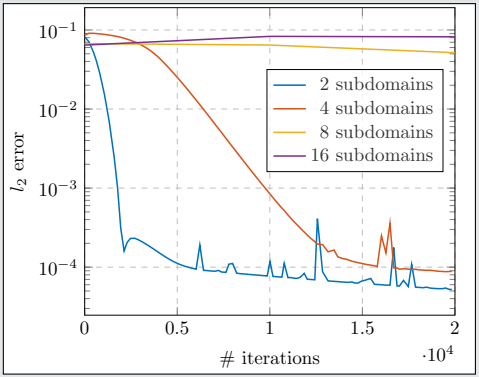

Two-Level FBPINNs

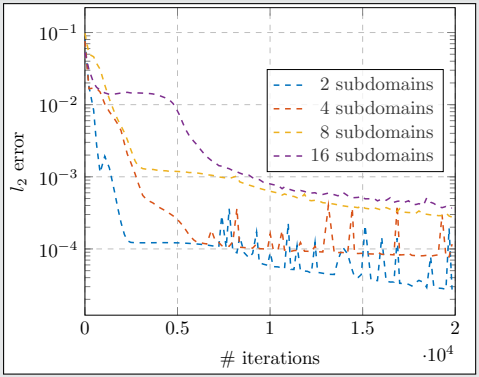

Multi-Level FBPINN Algorithm

We introduce a **hierarchy of L overlapping domain decompositions**

$$\Omega = \bigcup_{j=1}^{J^{(l)}} \Omega_j^{(l)}$$

and corresponding window functions $\omega_j^{(l)}$ with $\text{supp}\left(\omega_j^{(l)}\right) \subset \Omega_j^{(l)}$ and $\sum_{j=1}^{J^{(l)}} \omega_j^{(l)} \equiv 1$ on Ω.

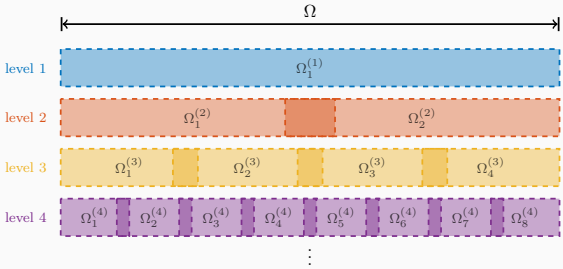

This yields the ***L*-level FBPINN algorithm**:

L-level network architecture

$$u\left(\theta_1^{(1)}, \ldots, \theta_{J^{(L)}}^{(L)}\right) = \mathcal{C}\left(\sum_{l=1}^{L} \sum_{i=1}^{N^{(l)}} \omega_j^{(l)} u_j^{(l)}\left(\theta_j^{(l)}\right)\right)$$

Loss function

$$\mathcal{L} = \frac{1}{N} \sum_{i=1}^{N} \left(\eta[\mathcal{C} \sum_{x_i \in \Omega_j^{(l)}} \omega_j^{(l)} u_j^{(l)}](x_i, \theta_j^{(l)}) - f(x_i)\right)^2$$

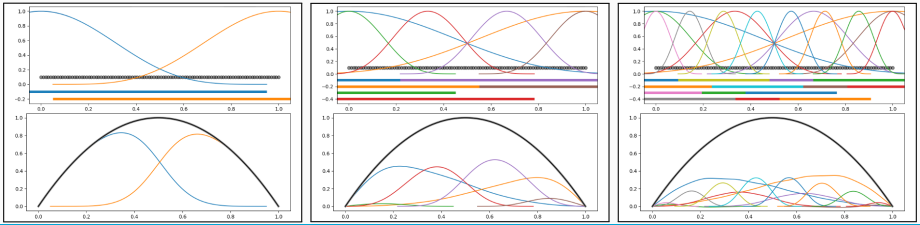

Multilevel FBPINNs – 2D Laplace

Let us now consider the **simple two-dimensional boundary value problem**

$$\begin{aligned} -\Delta u &= 32(x(1-x)+y(1-y)) && \text{in } \Omega = [0,1]^2, \\ u &= 0 && \text{on } \partial\Omega, \end{aligned}$$

which has the **solution**

$$u(x,y) = 16\,(x(1-x)y(1-y))\,.$$

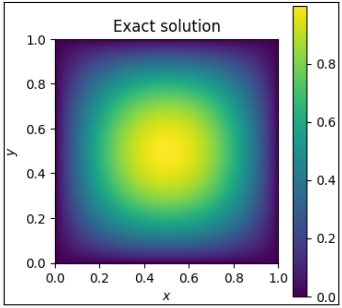

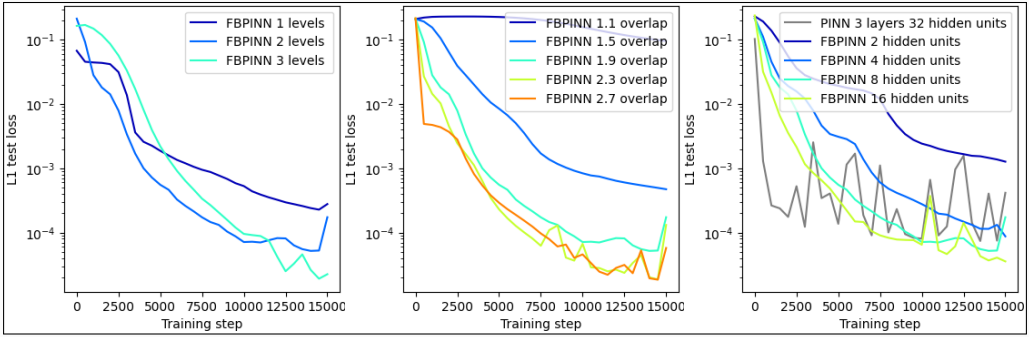

Multi-Level FBPINNs for a Multi-Frequency Problem – Strong Scaling

$$-\Delta u = 2\sum_{i=1}^{n} (\omega_i \pi)^2 \sin(\omega_i \pi \boldsymbol{x}) \sin(\omega_i \pi \boldsymbol{y}) \quad \text{in } \Omega = [0,1]^2,$$
$$u = 0 \quad \text{on } \partial\Omega.$$

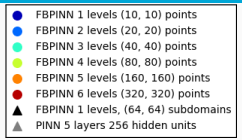

Strong scaling

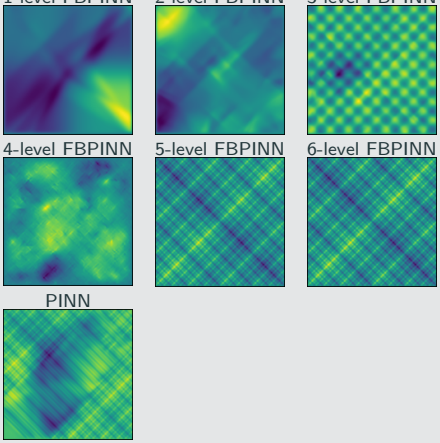

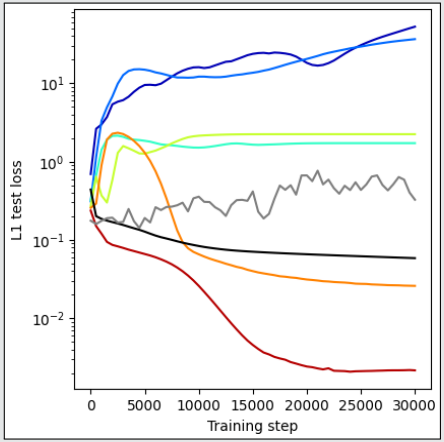

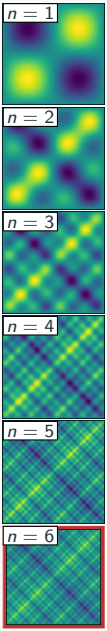

Multi-Level FBPINNs for a Multi-Frequency Problem – Strong Scaling

$$-\Delta u = 2\sum_{i=1}^{n} (\omega_i \pi)^2 \sin(\omega_i \pi \boldsymbol{x}) \sin(\omega_i \pi \boldsymbol{y}) \quad \text{in } \Omega = [0,1]^2,$$
$$u = 0 \quad \text{on } \partial\Omega.$$

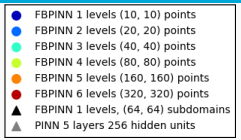

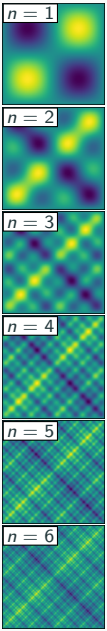

Weak scaling

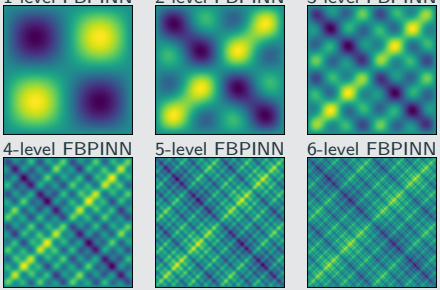

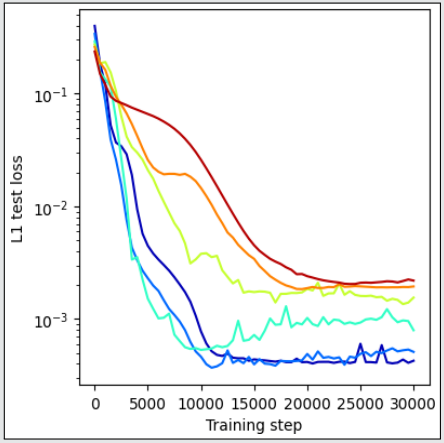

Surrogate models for computational fluid dynamics simulations

Computational Fluid Dynamics (CFD) Simulations are Time Consuming

In Giese, Heinlein, Klawonn, Knepper, Sonnabend (2019), a benchmark for **comparing MRI measurements and CFD simulations** of hemodynamics in **intracranial aneurysms** was proposed.

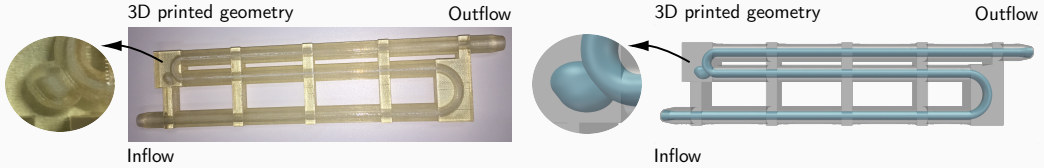

To obtain accurate simulation results, a simulation with $\approx 10\,\mathrm{m}$ d.o.f.s has been carried out. On $O(100)$ MPI ranks, the computation of a steady state took $O(1)\,\mathrm{h}$ on CHEOPS supercomputer at UoC.

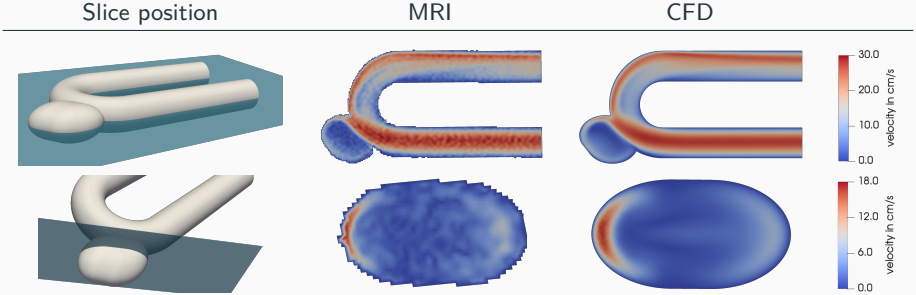

Computational Fluid Dynamics (CFD) Simulations are Time Consuming

In Giese, Heinlein, Klawonn, Knepper, Sonnabend (2019), a benchmark for **comparing MRI measurements and CFD simulations** of hemodynamics in **intracranial aneurysms** was proposed.

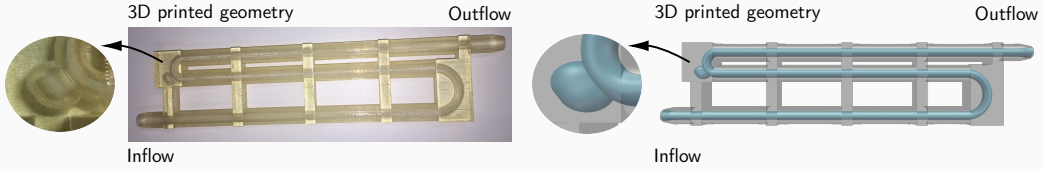

To obtain accurate simulation results, a simulation with $\approx 10\,\mathrm{m}$ d.o.f.s has been carried out. On $O(100)$ MPI ranks, the computation of a steady state took $O(1)\,\mathrm{h}$ on CHEOPS supercomputer at UoC.

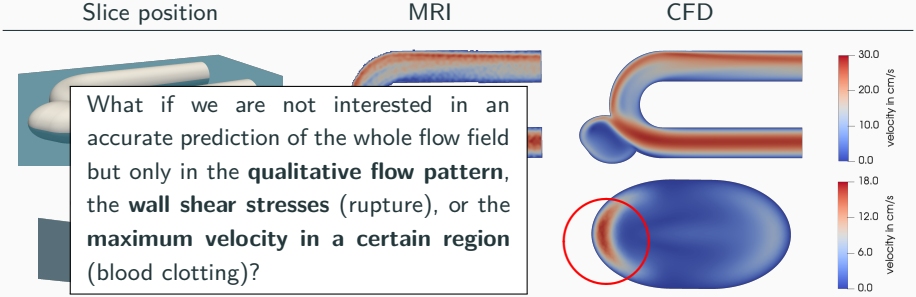

What if we are not interested in an accurate prediction of the whole flow field but only in the **qualitative flow pattern**, the **wall shear stresses** (rupture), or the **maximum velocity in a certain region** (blood clotting)?

Operator Learning and Surrogate Modeling

Our approach is inspired by the work Guo, Li, Iorio (2016), in which **convolutional neural networks (CNNs)** are employed to predict the flow in channel with an obstacle.

In particular, we use a pixel image of the **geometry as input** and predict an image of the resulting **stationary flow field as output**:

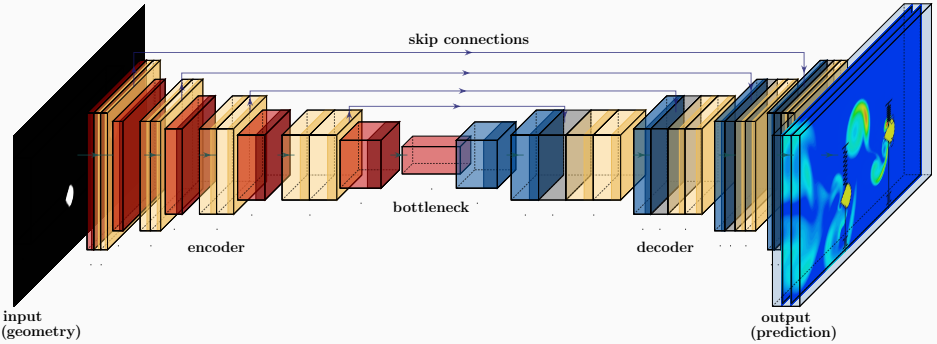

Other related works: E.g.

- Guo, Li, Iorio (2016)
- Niekamp, Niemann, Schröder (2022)
- Stender, Ohlsen, Geisler, Chabchoub, Hoffmann, Schlaefer (2022)

Operator Learning and Surrogate Modeling

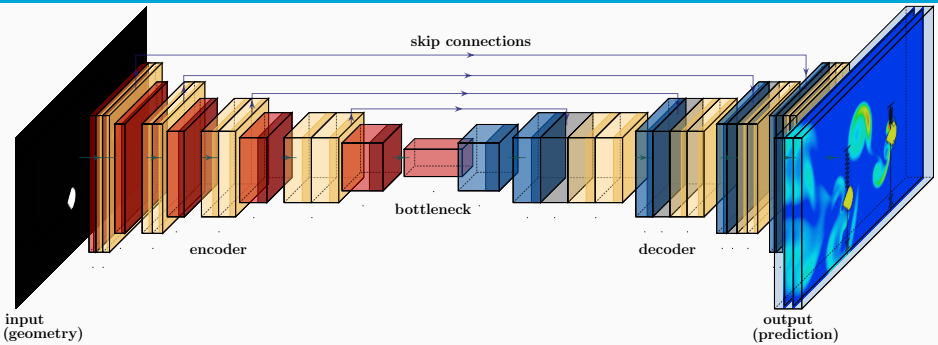

We learn the **nonlinear map** between a **representation space of the geometry** and the **solution space** of the stationary Navier–Stokes equations → **Operator learning**.

Operator learning

Learning **maps between function spaces**, e.g.,

- between the right-hand side and the solution of a BVP.

Other operator learning approaches

- **DeepOnet:** Lu, Jin, and Karniadakis. (arXiv preprint 2019).
- **Neural operators:** Kovachki, Li, Liu, Azizzadenesheli, Bhattacharya, Stuart, and Anandkumar (arXiv preprint 2021).

Model Problem – Flow Around an Obstacle in Two Dimensions

We propose a **simple model problem** to investigate predictions of a **steady flow in a channel with an obstacle**; this setup is also inspired by **Guo, Li, Iorio (2016)**.

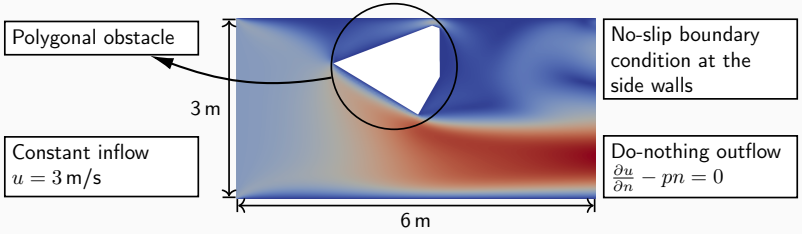

Data: randomly generated geometries (star-shaped polygons with 3, 4, 5, 6, and 12 edges)

type I (50 k configurations)

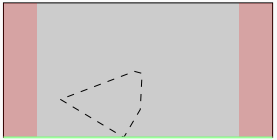

type II (50 k configurations)

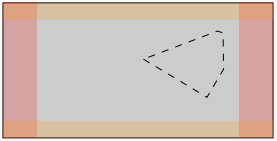

type III

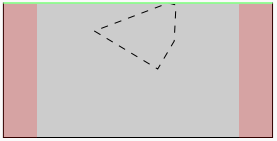

90 k training data & 10 k test data

(transfer learning; cf. **Eichinger, Heinlein, Klawonn (2022)**)

Computation of the Flow Data Using OpenFOAM®

We solve the **steady Navier–Stokes equations**

$$-\nu\Delta\vec{u} + (u\cdot\nabla)\,\vec{u} + \nabla p = 0 \text{ in } \Omega,$$
$$\nabla\cdot u = 0 \text{ in } \Omega,$$

where $\vec{u}$ and p are the velocity and pressure fields and ν is the viscosity. Furthermore, we prescribe the previously described boundary conditions.

Software pipeline

1. Define the boundary of the polygonal obstacle and **create the corresponding STL (standard triangulation language) file**.
2. **Generate a hexahedral compute grid** (`snappyHexMesh`).
3. Run the **CFD simulation** (`simpleFoam`).
4. **Interpolate geometry information and flow field** onto a pixel grid.
5. **Train the CNN**.

Input data

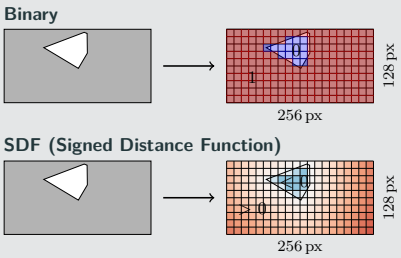

Output data

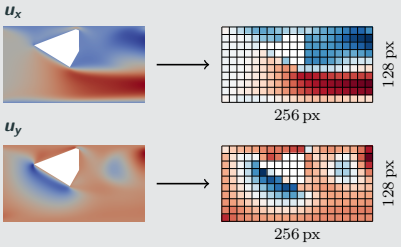

Neural Network Architectures

Bottleneck CNN (Guo, Li, Iorio (2016))

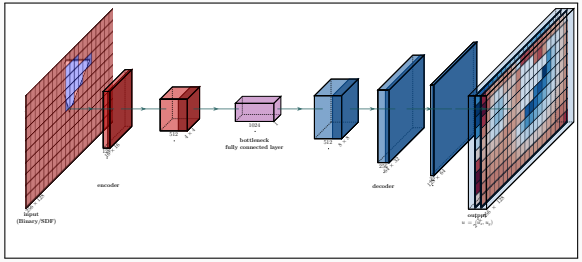

U-Net (Ronneberger, Fischer, Brox (2015))

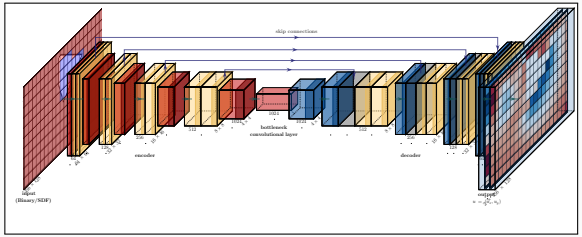

One decoder

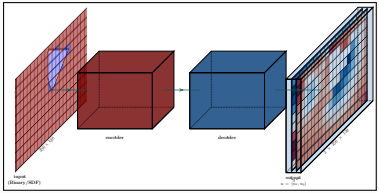

Two decoders

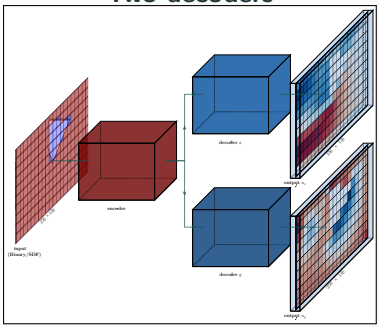

Comparison CFD Vs NN (Relative Error 2 %)

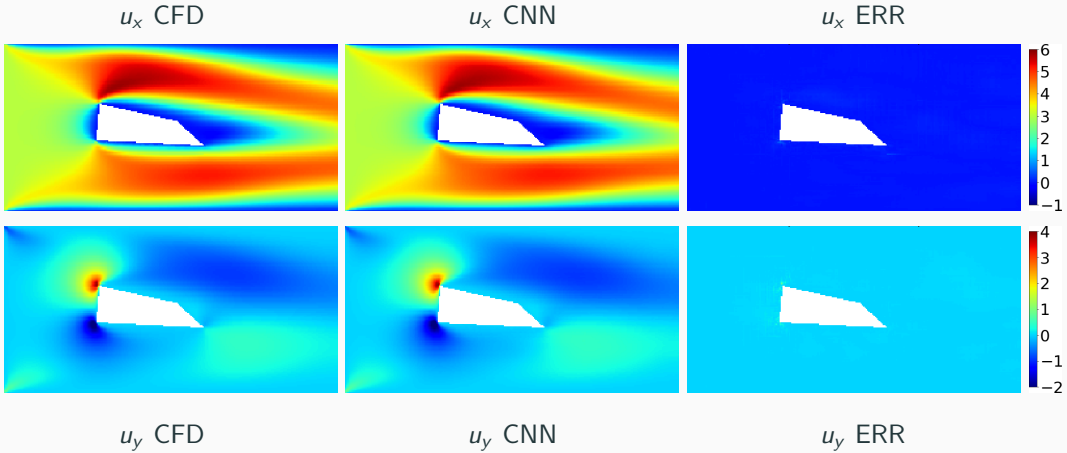

Cf. **Eichinger, Heinlein, Klawonn (2021, 2022)**

Comparison CFD Vs NN (Relative Error 14 %)

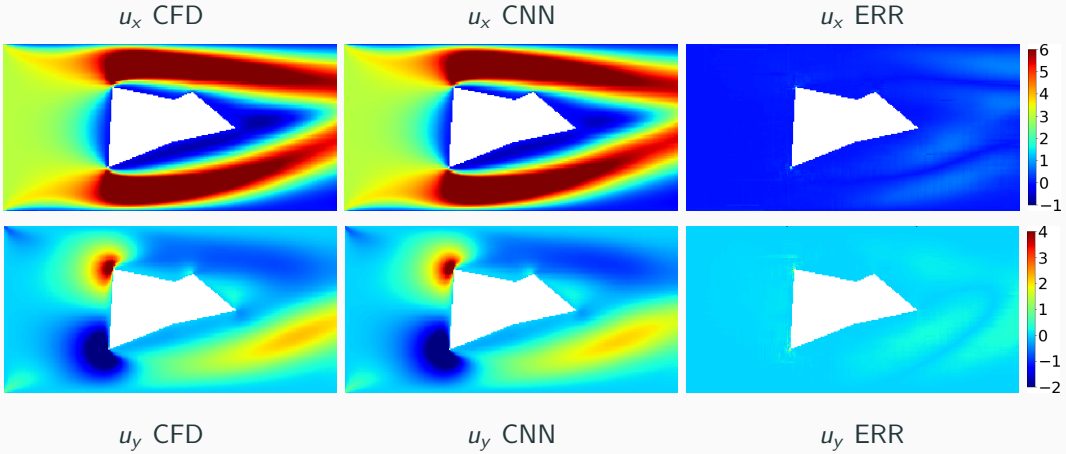

Cf. **Eichinger, Heinlein, Klawonn (2021, 2022)**

Comparison CFD Vs NN (Relative Error 31 %)

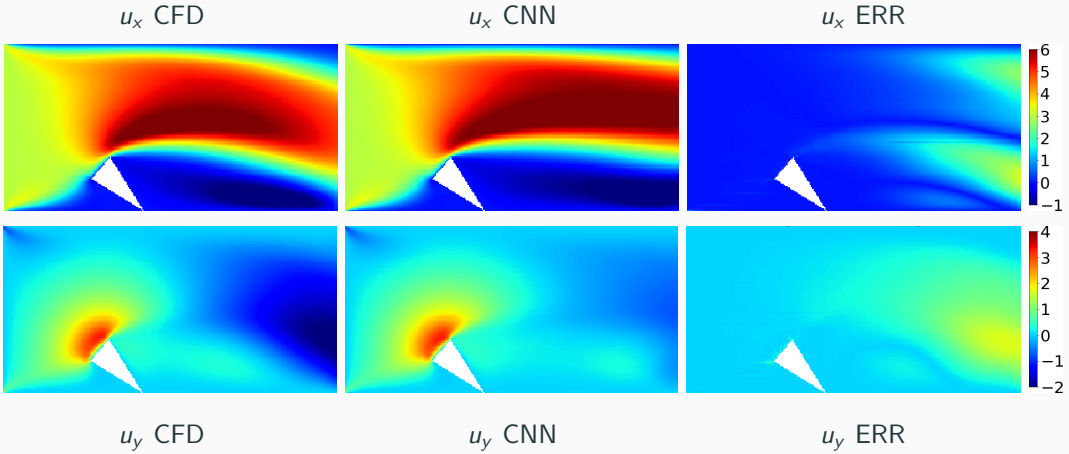

Cf. **Eichinger, Heinlein, Klawonn (2021, 2022)**

First Results (Eichinger, Heinlein, Klawonn (2021, 2022))

We compare the **relative error (RE)** $\frac{\|u_{i,j} - \hat{u}_{i,j}\|_2}{\|u_{i,j}\|_2 + 10^{-4}}$ **averaged over all non-obstacle pixels** and **all validation data configurations**. Furthermore: **MSE = mean squared error**; **MAE = mean absolute error**.

			Bottleneck CNN (Guo, Li, Iorio (2016))			**U-Net (Ronneberger, Fischer, Brox (2015))**		
input	# dec.	loss	total	type I	type II	total	type I	type II
SDF	1	MSE	**61.16 %**	110.46 %	11.86 %	17.04 %	29.42 %	4.66 %
		MSE + RE	3.97 %	3.31 %	**4.63 %**	2.67 %	2.11 %	3.23 %
		MAE	25.19 %	41.52 %	8.86 %	9.10 %	13.89 %	4.32 %
		MAE + RE	4.45 %	3.84 %	5.05 %	2.48 %	1.87 %	**3.10 %**
	2	MSE	49.82 %	89.12 %	10.51 %	13.01 %	21.59 %	4.42 %
		MSE + RE	**3.85 %**	**3.05 %**	4.64 %	**2.43 %**	**1.78 %**	3.23 %
		MAE	45.23 %	81.38 %	9.08 %	5.47 %	7.06 %	3.89 %
		MAE + RE	4.33 %	3.74 %	4.91 %	2.57 %	1.98 %	3.17 %
Binary	1	MSE	49.78 %	88.28 %	11.28 %	27.15 %	49.15 %	5.15 %
		MSE + RE	10.12 %	11.44 %	8.80 %	5.49 %	6.25 %	4.74 %
		MAE	39.16 %	64.77 %	13.54 %	15.69 %	26.36 %	5.02 %
		MAE + RE	10.61 %	12.34 %	8.87 %	**4.48 %**	**5.05 %**	**3.90 %**
	2	MSE	**51.34 %**	91.20 %	11.48 %	24.00 %	43.14 %	4.85 %
		MSE + RE	10.03 %	11.37 %	8.69 %	5.56 %	6.79 %	4.33 %
		MAE	37.16 %	62.01 %	12.32 %	21.54 %	38.12 %	4.96 %
		MAE + RE	**9.53 %**	**10.91 %**	**8.15 %**	6.04 %	7.88 %	4.20 %

Generalization Properties (Eichinger, Heinlein, Klawonn (2021, 2022))

We test the **generalization properties** of our **previously trained U-Net**. In particular, we predict the flow for new geometries of **Type I** and **Type II**; 1 000 geometries each (500 Type I & 500 Type II).

# polygon edges	SDF input			Binary input		
	total	type I	type II	total	type I	type II
7	2.71 %	1.89 %	3.53 %	4.39 %	4.61 %	4.16 %
8	2.82 %	1.98 %	3.65 %	4.67 %	4.89 %	4.44 %
10	3.21 %	2.32 %	4.10 %	5.23 %	5.51 %	4.94 %
15	4.01 %	3.16 %	4.86 %	7.76 %	7.85 %	6.66 %
20	5.08 %	4.22 %	5.93 %	9.70 %	10.43 %	8.97 %

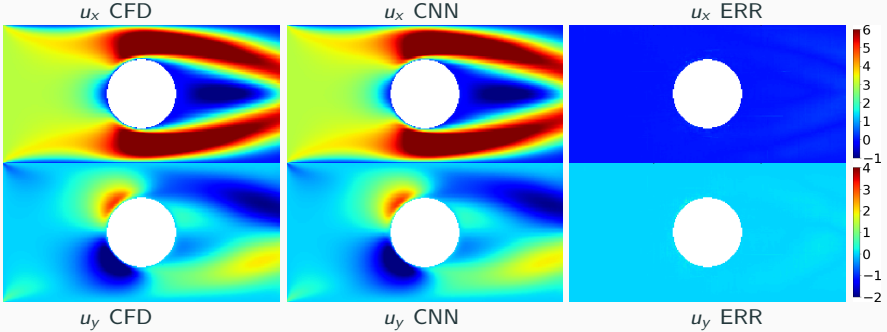

Generalization Issues – Type III Geometry (Relative Error 158 %)

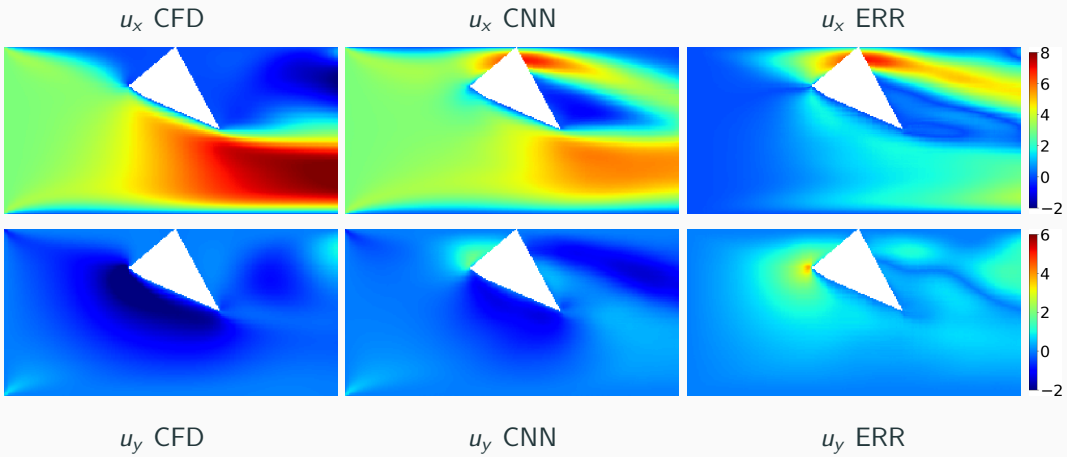

Cf. **Eichinger, Heinlein, Klawonn (2022)**

Transfer Learning – Type III Geometries

The **best model (U-Net, one decoder, MAE+RE loss)** trained on type I and type II geometries **performs poorly on 2 500 type III geometries**:

	SDF Input	binary Input
type III	22 985.89 %	4 134.69 %

We compare the following approaches to generalize to type III geometries:

- **Approach 1:** Train a new model from scratch on type III geometries (2 500 training + 2 500 validation data)
- **Approach 2:** Train the previous model on type III geometries
- **Approach 3:** Train the previous model on a data set consisting of the old data (type I & type II) and type III data

		type I & II		type III	
learning approach	# training epochs	SDF input	binary input	SDF input	binary input
1	100	-	-	98.02 %	111.75 %
2	100	208.02 %	105.43 %	7.18 %	11.81 %
3	3	**3.33 %**	**7.06 %**	**4.94 %**	**11.28 %**

Neural networks **forget if data is removed from the training data**. However, **new geometries (type III: symmetric to Type I) can be learned quickly** if they are **added to the existing training data**.

Computing Times

Data:

	Avg. Runtime per Case (Serial)
Create STL	0.15 s
`snappyHexMesh`	37 s
`simpleFoam`	13 s
Total Time	$\approx$ 50 s

Training:

	Bottleneck CNN		**U-Net**	
# decoders	1	2	1	2
# parameters	$\approx$ 47 m	$\approx$ 85 m	$\approx$ 34 m	$\approx$ 53.5 m
time/epoch	**180 s**	**245 s**	**195 s**	**270 s**

Comparison CFD Vs NN:

	CFD (CPU)	**NN (CPU)**	**NN (GPU)**
Avg. Time	**50 s**	**0.092 s**	**0.0054 s**

$\Rightarrow$ Flow predictions using neural networks may be less accurate and the **training phase expensive**, but the **flow prediction is** $\approx 5 \cdot 10^2 - 10^4$ **times faster**.

CPU: AMD Threadripper 2950X (8 $\times$ 3.8 Ghz), 32GB RAM; **GPU:** GeForce RTX 2080Ti

U-Net Revisited & Action of a Discrete Convolution

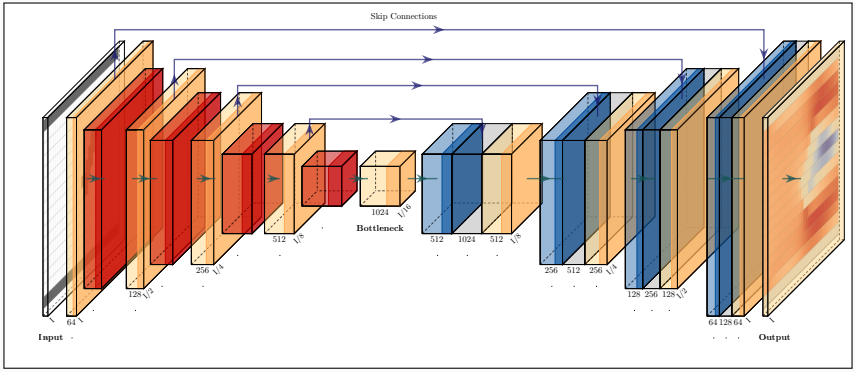

Convolution

The action of a **convolutional layer** corresponds to **going over the image with a filter** (matrix):

$$\begin{pmatrix} a_{11} & a_{12} & a_{13} \\ a_{21} & a_{22} & a_{23} \\ a_{31} & a_{32} & a_{33} \end{pmatrix}$$

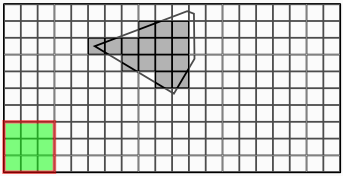

U-Net Revisited & Action of a Discrete Convolution

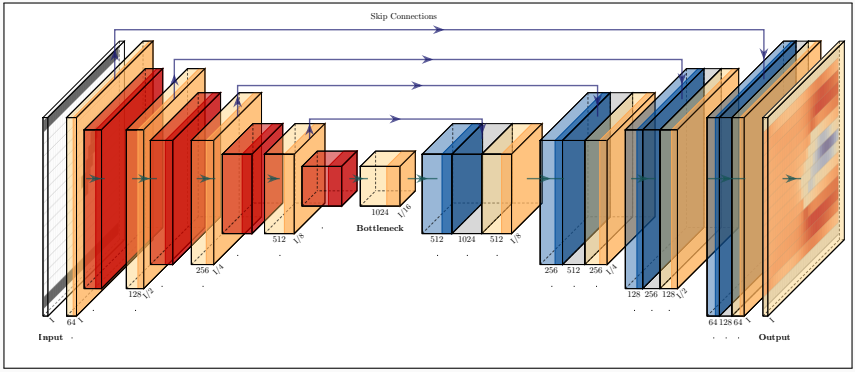

Convolution

The action of a **convolutional layer** corresponds to **going over the image with a filter** (matrix):

$$\begin{pmatrix} a_{11} & a_{12} & a_{13} \\ a_{21} & a_{22} & a_{23} \\ a_{31} & a_{32} & a_{33} \end{pmatrix}$$

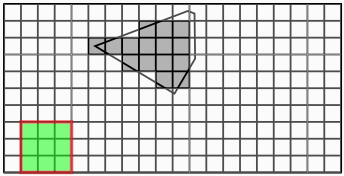

U-Net Revisited & Action of a Discrete Convolution

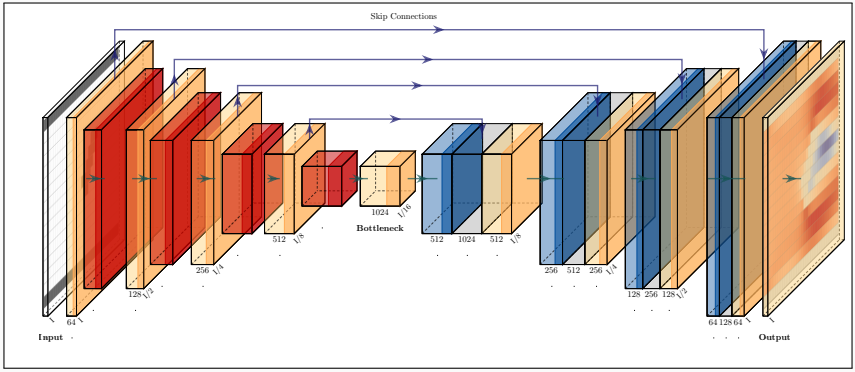

Convolution

The action of a **convolutional layer** corresponds to **going over the image with a filter** (matrix):

$$\begin{pmatrix} a_{11} & a_{12} & a_{13} \\ a_{21} & a_{22} & a_{23} \\ a_{31} & a_{32} & a_{33} \end{pmatrix}$$

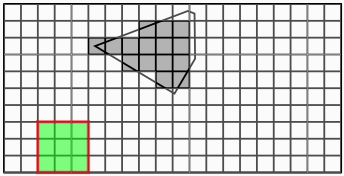

Unsupervised Learning Approach – PDE Loss Using Finite Differences

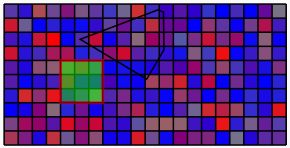

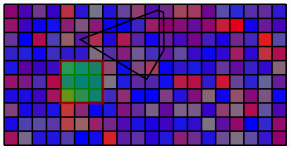

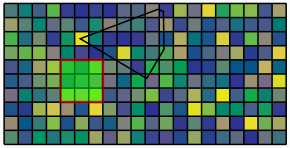

$$\left\| \begin{matrix} F_{\text{mom}}(u_{\text{NN}}, p_{\text{NN}}) \\ F_{\text{mass}}(u_{\text{NN}}, p_{\text{NN}}) \end{matrix} \right\|^2 >> 0$$

Minimization of the mean squared residual of the Navier-Stokes equations

$$\min_{u_{\text{NN}}, p_{\text{NN}}} \frac{1}{\#\text{pixels}} \sum_{\text{pixels}} \left\| \begin{matrix} F_{\text{mom}}(u_{\text{NN}}, p_{\text{NN}}) \\ F_{\text{mass}}(u_{\text{NN}}, p_{\text{NN}}) \end{matrix} \right\|^2$$

where u_{NN} and p_{NN} are the output images of our CNN and

$$\begin{aligned} F_{\text{mom}}(u, p) &:= -\nu \Delta \vec{u} + (u \cdot \nabla)\, \vec{u} + \nabla p, \\ F_{\text{mass}}(u, p) &:= \nabla \cdot u. \end{aligned}$$

We use a **finite difference discretization on the output pixel image** by defining filters on the last layer of the CNN-based on the stencils:

$\frac{\partial}{\partial x}$

$$\begin{matrix} 0 & 0 & 0 \\ -1 & 0 & 1 \\ 0 & 0 & 0 \end{matrix}$$

$$\begin{matrix} 0 & 1 & 0 \\ 0 & 0 & 0 \\ 0 & -1 & 0 \end{matrix}$$

$\frac{\partial}{\partial y}$

$\frac{\partial^2}{\partial x^2}$

$$\begin{matrix} 0 & 0 & 0 \\ 1 & -2 & 1 \\ 0 & 0 & 0 \end{matrix}$$

$$\begin{matrix} 0 & 1 & 0 \\ 0 & -2 & 0 \\ 0 & 1 & 0 \end{matrix}$$

$\frac{\partial^2}{\partial y^2}$

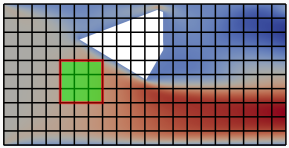

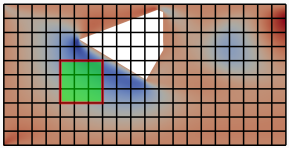

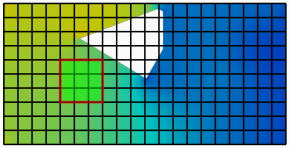

$$\left\| \begin{matrix} F_{\text{mom}}(u_{\text{NN}}, p_{\text{NN}}) \\ F_{\text{mass}}(u_{\text{NN}}, p_{\text{NN}}) \end{matrix} \right\|^2 \approx 0$$

Cf. **Grimm, Heinlein, Klawonn**

Physics-Informed Approach & Boundary Conditions

The PDE loss can be minimized **without using simulation results as training data**.

→ On a single geometry, this training of the neural network just corresponds to an **unconventional way of solving the Navier-Stokes equations using finite differences**.

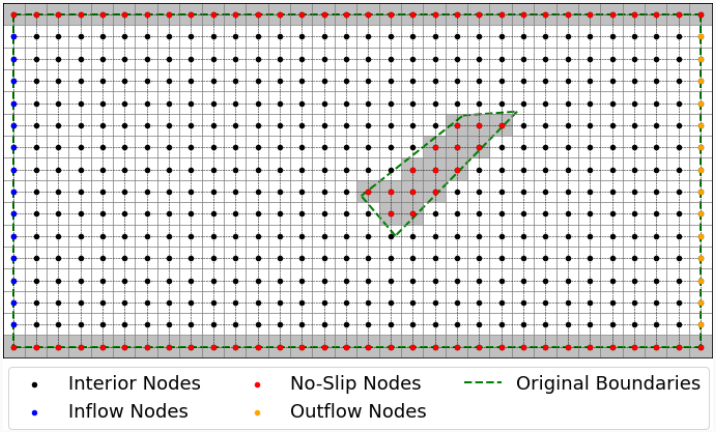

Boundary conditions

- Computing the correct solution requires **enforcing the correct boundary conditions**.
- Therefore, we additionally encode **flags for the different boundary conditions** in the **input image**.

Physics-Informed Approach – Single Geometry

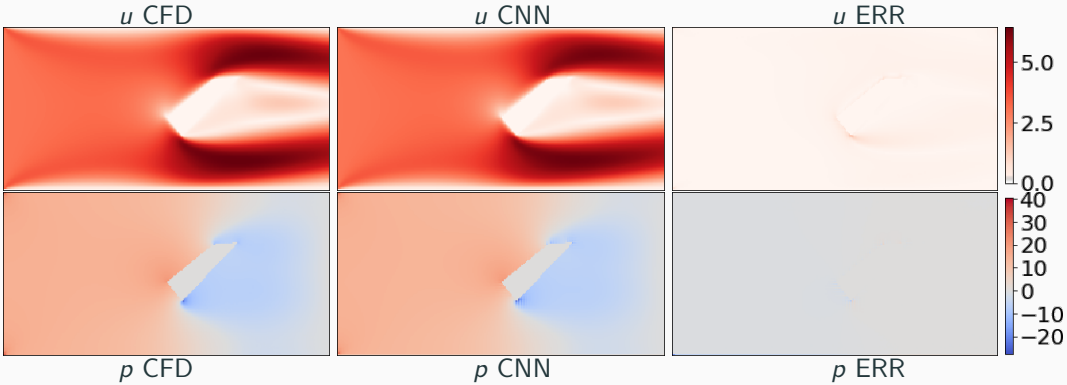

Physics-Informed Approach – Single Geometry

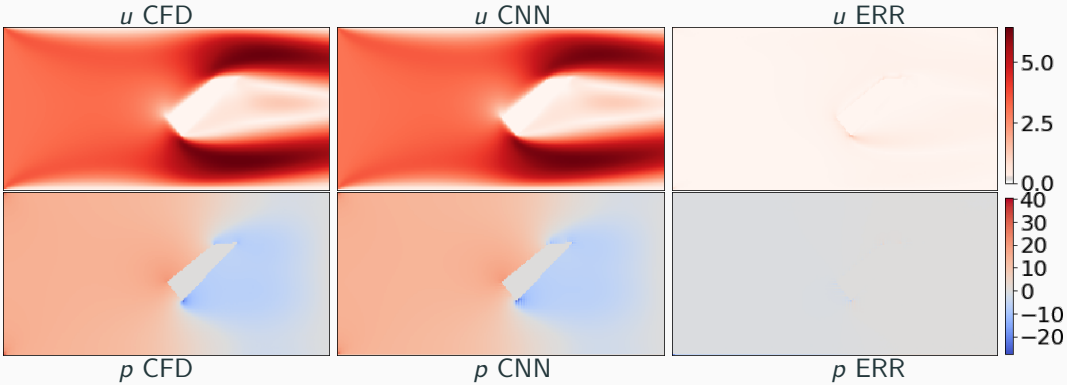

⇒ We can **solve the boundary value problem using a neural network**. Let us briefly discuss why, for a **single geometry**, this is **not an efficient solver**.

Convergence Comparison – CNN Versus FDM

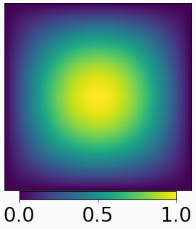

Solve

$$-\Delta u = f$$

using

- classical finite differences
- **ML**: CNN
- **GD**: gradient descent
- **CG**: conjugate gradient method
- **SE**: $Ax = b$
- **NE**: $\|Ax - b\|^2$

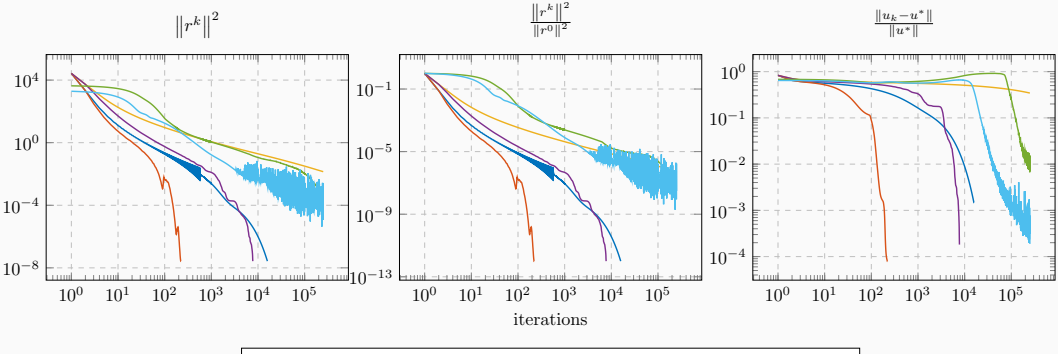

Convergence Comparison – CNN Versus FDM

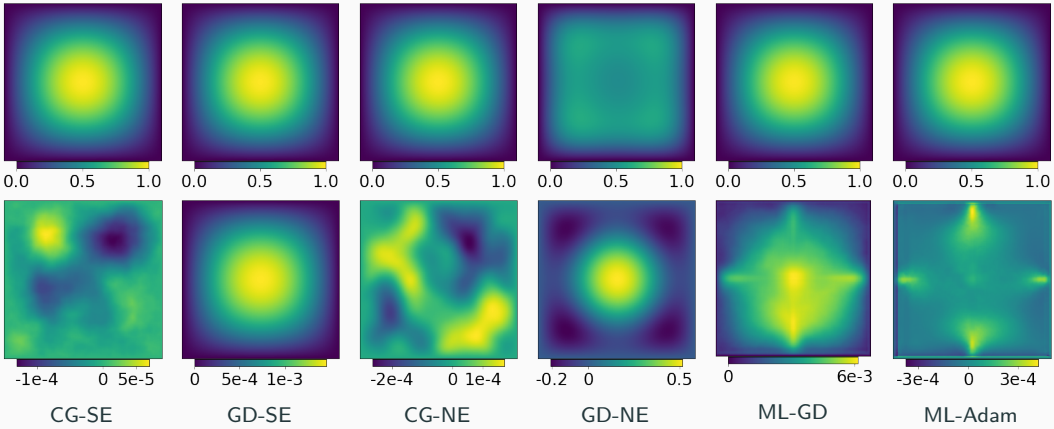

The results are in alignment with the **spectral bias of neural networks**. The neural network approximations yield a low error norm compared with the residual (MSE loss).

$$Ae = A(u^* - u) = b - Au = r$$

Cf. **Grimm, Heinlein, Klawonn (submitted 2022)**.

Convergence Comparison – CNN Versus FDM

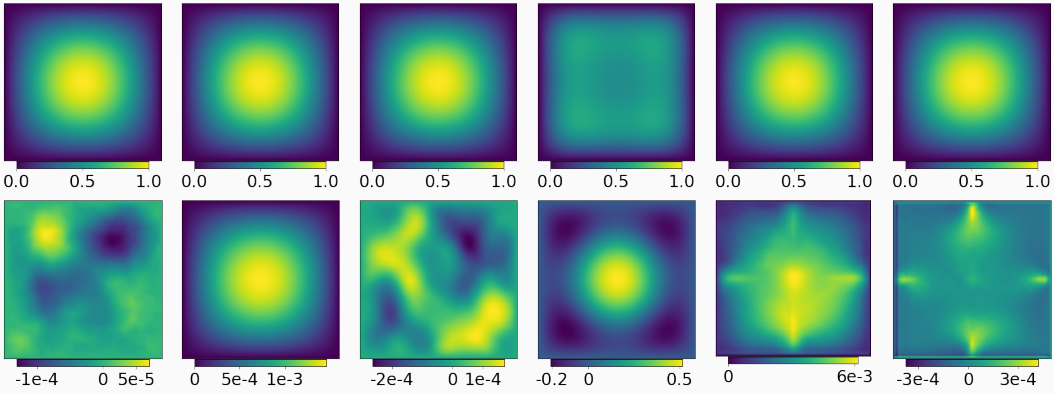

The results are in alignment with the **spectral bias of neural networks**. The neural network approximations yield a low error norm compared with the residual (MSE loss).

$$Ae = A(u^* - u) = b - Au = r$$

Cf. **Grimm, Heinlein, Klawonn (submitted 2022).**

→ **Next:** surrogate model for multiple geometries

Results on $\approx 5\,000$ Type II Geometries

	training data	error	$\frac{\|u_{NN}-u\|_2}{\|u\|_2}$	$\frac{\|p_{NN}-p\|_2}{\|p\|_2}$	mean residual momentum	mean residual mass	# epochs trained
data-based	10%	train.	2.07%	10.98%	$1.1 \cdot 10^{-1}$	$1.4 \cdot 10^{0}$	500
		val.	4.48 %	15.20 %	$1.6 \cdot 10^{-1}$	$1.7 \cdot 10^{0}$	
	25%	train.	1.93%	8.45%	$9.1 \cdot 10^{-2}$	$1.2 \cdot 10^{0}$	500
		val.	3.49 %	10.70 %	$1.2 \cdot 10^{-1}$	$1.4 \cdot 10^{0}$	
	50%	train.	1.48%	8.75%	$9.0 \cdot 10^{-2}$	$1.1 \cdot 10^{0}$	500
		val.	2.70 %	10.09 %	$1.1 \cdot 10^{-1}$	$1.2 \cdot 10^{0}$	
	75%	train.	1.43%	7.30%	$1.0 \cdot 10^{-1}$	$1.5 \cdot 10^{0}$	500
		val.	**2.52 %**	**8.67 %**	$1.2 \cdot 10^{-1}$	$1.5 \cdot 10^{0}$	
physics-informed	10%	train.	5.35%	12.95%	$3.5 \cdot 10^{-2}$	$7.8 \cdot 10^{-2}$	**5 000**
		val.	6.72%	15.39%	$6.7 \cdot 10^{-2}$	$2.0 \cdot 10^{-1}$	
	25%	train.	5.03%	12.26%	$3.2 \cdot 10^{-2}$	$7.3 \cdot 10^{-2}$	**5 000**
		val.	5.78 %	13.38 %	$5.3 \cdot 10^{-2}$	$1.4 \cdot 10^{-1}$	
	50%	train.	5.81%	12.92%	$3.9 \cdot 10^{-2}$	$9.3 \cdot 10^{-2}$	**5 000**
		val.	5.84 %	12.73 %	$4.8 \cdot 10^{-2}$	$1.2 \cdot 10^{-1}$	
	75%	train.	5.03%	11.63%	$3.2 \cdot 10^{-2}$	$7.7 \cdot 10^{-2}$	**5 000**
		val.	**5.18 %**	**11.60 %**	$4.2 \cdot 10^{-2}$	$1.1 \cdot 10^{-1}$	

Results on $\approx$ 5 000 Type II Geometries

	training data	error	$\frac{\|u_{NN}-u\|_2}{\|u\|_2}$	$\frac{\|p_{NN}-p\|_2}{\|p\|_2}$	mean residual momentum	mean residual mass	# epochs trained
data-based	10%	train.	2.07%	10.98%	$1.1 \cdot 10^{-1}$	$1.4 \cdot 10^{0}$	500
		val.	4.48 %	15.20 %	$1.6 \cdot 10^{-1}$	$1.7 \cdot 10^{0}$	
	25%	train.	1.93%	8.45%	$9.1 \cdot 10^{-2}$	$1.2 \cdot 10^{0}$	500
		val.	3.49 %	10.70 %	$1.2 \cdot 10^{-1}$	$1.4 \cdot 10^{0}$	
	50%	train.	1.48%	8.75%	$9.0 \cdot 10^{-2}$	$1.1 \cdot 10^{0}$	500
		val.	2.70 %	10.09 %	$1.1 \cdot 10^{-1}$	$1.2 \cdot 10^{0}$	
	75%	train.	1.43%	7.30%	$1.0 \cdot 10^{-1}$	$1.5 \cdot 10^{0}$	500
		val.	**2.52 %**	**8.67 %**	$1.2 \cdot 10^{-1}$	$1.5 \cdot 10^{0}$	
physics-informed	10%	train.	5.35%	12.95%	$3.5 \cdot 10^{-2}$	$7.8 \cdot 10^{-2}$	**5 000**
		val.	6.72%	15.39%	$6.7 \cdot 10^{-2}$	$2.0 \cdot 10^{-1}$	
	25%	train.	5.03%	12.26%	$3.2 \cdot 10^{-2}$	$7.3 \cdot 10^{-2}$	**5 000**
		val.	5.78 %	13.38 %	$5.3 \cdot 10^{-2}$	$1.4 \cdot 10^{-1}$	
	50%	train.	5.81%	12.92%	$3.9 \cdot 10^{-2}$	$9.3 \cdot 10^{-2}$	**5 000**
		val.	5.84 %	12.73 %	$4.8 \cdot 10^{-2}$	$1.2 \cdot 10^{-1}$	
	75%	train.	5.03%	11.63%	$3.2 \cdot 10^{-2}$	$7.7 \cdot 10^{-2}$	**5 000**
		val.	**5.18 %**	**11.60 %**	$4.2 \cdot 10^{-2}$	$1.1 \cdot 10^{-1}$	

$\rightarrow$ The results for the **physics-informed approach** are **comparable to the data-based approach**; the **errors are slightly higher**. However, no **reference data at all is needed for the training**.

Generalization

Now, consider an obstacle which is **closer to the wall** ($\approx 0.4\,\mathrm{m}$) **than the training data** ($\geq 0.75\,\mathrm{m}$).

Supervised approach

$$\frac{\|u_{NN} - u\|_2}{\|u\|_2} = 23\%$$

$$\frac{\|p_{NN} - p\|_2}{\|p\|_2} = 31\%$$

Unsupervised approach

$$\frac{\|u_{NN} - u\|_2}{\|u\|_2} = 14\%$$

$$\frac{\|p_{NN} - p\|_2}{\|p\|_2} = 27\%$$

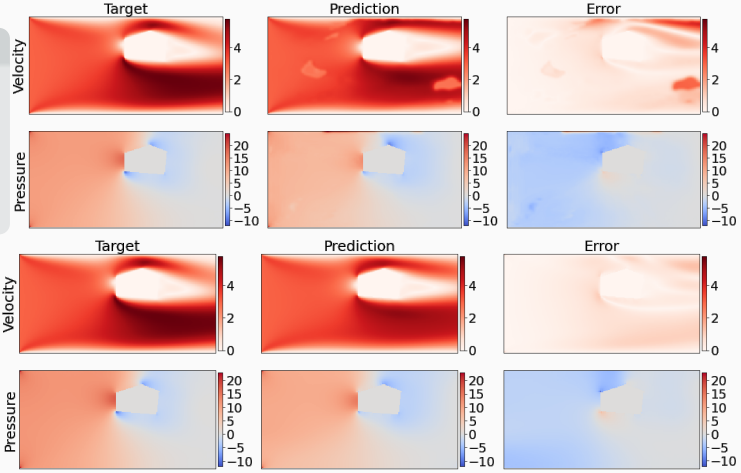

Generalization

Now, consider an obstacle which is **closer to the wall** ($\approx 0.4\,\mathrm{m}$) **than the training data** ($\geq 0.75\,\mathrm{m}$).

Supervised approach

$$\frac{\|u_{NN} - u\|_2}{\|u\|_2} = 23\%$$

$$\frac{\|p_{NN} - p\|_2}{\|p\|_2} = 31\%$$

Unsupervised approach

$$\frac{\|u_{NN} - u\|_2}{\|u\|_2} = 14\%$$

$$\frac{\|p_{NN} - p\|_2}{\|p\|_2} = 27\%$$

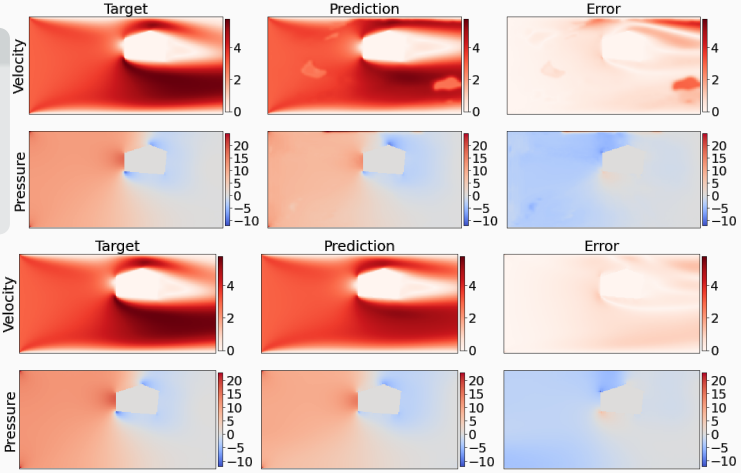

→ The unsupervised approach **generalizes slightly better**, and in particular, **the prediction is smoother and misses unphysical artifacts**.

Generalization With Respect to the Inflow Velocity

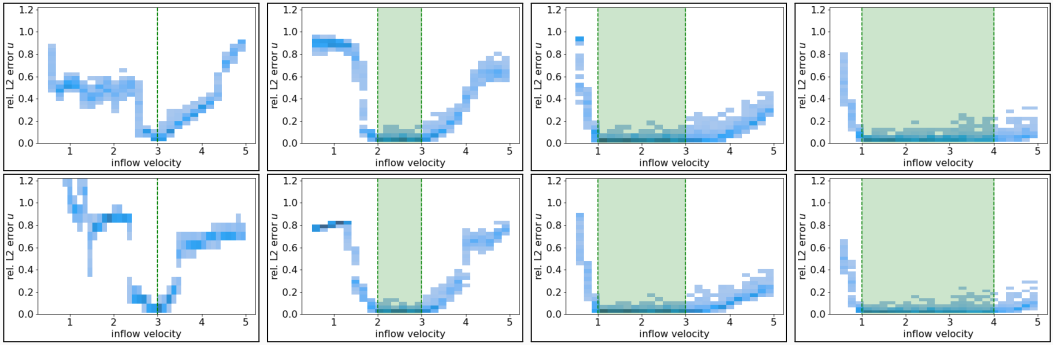

order	# data	range inflow vel.	[0.5, 1.0]	[1.0, 2.0]	[2.0, 3.0]	[3.0, 4.0]	[4.0, 5.0]
2	1 000	[3.0, 3.0]	55.5 %	48.1 %	31.1 %	17.4 %	61.5 %
		[2.0, 3.0]	89.3 %	57.4 %	**4.0 %**	15.5 %	59.1 %
		[1.0, 3.0]	40.2 %	**3.8 %**	**4.3 %**	7.1 %	20.4 %
		[1.0, 4.0]	31.3 %	**4.0 %**	**4.3 %**	**5.8 %**	7.7 %
2	4 500	[3.0, 3.0]	186.8 %	87.1 %	40.5 %	36.9 %	70.6 %
		[2.0, 3.0]	78.4 %	44.3 %	**3.2 %**	16.1 %	68.2 %
		[1.0, 3.0]	38.7 %	**2.9 %**	**3.4 %**	6.7 %	18.5 %
		[1.0, 4.0]	27.7 %	**3.1 %**	**3.4 %**	**4.7 %**	7.2 %

Aneurysm Geometries

Training: 500 geometries **Validation:** $\approx$ 1 200 geometries

Relative $L2$**-error** on the **validation data set** in u: **4.9** %, in p: **9.5** %.

u: 3.3%, p: 7.4%

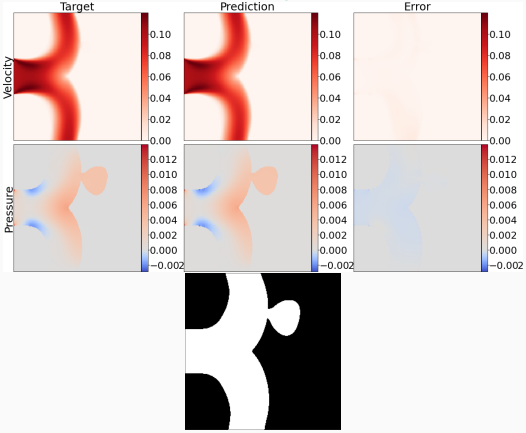

u: 13.2%, p: 35.1%

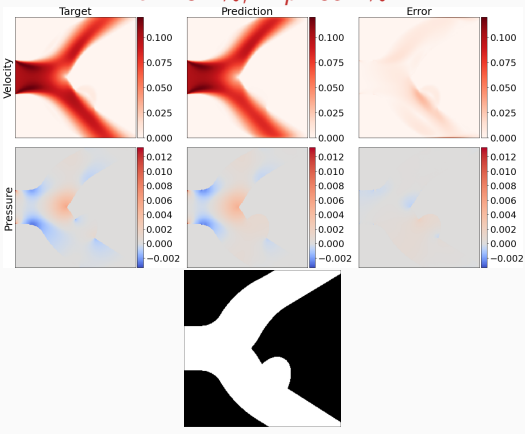

Summary

Scientific machine learning

- The field of **scientific machine learning (SciML)** deals with the **combination of scientific computing and machine learning** techniques; **physics-informed machine learning** models allow for the **combination of physical models and data**.

Finite basis physics-informed neural networks

- **Schwarz domain decomposition methods** can help to **improve the performance of PINNs**, especially for (but not restricted to) **large domains** and/or **multiscale problems**.

Surrogate models

- **CNNs** yield an **operator learning approach for predicting fluid flow** inside **varying computational domains**; the model can be trained using **data and/or physics**.

Acknowledgements

- The **Helmholtz School for Data Science in Life, Earth and Energy (HDS-LEE)**

Thank you for your attention!